Molecular Biology and Evolution, 2026, 43, 1–16
https://doi.org/10.1093/molbev/msag006
Published: 9 January 2026
Discoveries

MBE OXFORD

Genomic comparisons and the adaptive basis of brain size plasticity and chromosomal instability in the Eurasian common shrew

William R. Thomas [1†*], Tanya M. Lama [1,2], Cecilia Baldoni [3,4], Laia Marín-Gual [5,6], Diana Moreno Santillán [7], Marta Farré [8], Linelle Abueg [9], Jennifer Balacco [9], Olivier Fedrigo [9], Giulio Formenti [9], Nivesh Jain [9], Jacquelyn Mountcastle [9], Tatiana Tilley [9], Ying Sims [10], Alan Tracey [10], Jo Wood [10], David A. Ray [11], Dominik von Elverfeldt [12], John Nieland [13], Angelique P. Corthals [14], Aurora Ruiz-Herrera [5,6], Dina K.N. Dechmann [3,4], Erich Jarvis [9,15], Liliana M. Dávalos [1,16*]

[1]Department of Ecology and Evolution, Stony Brook University, Stony Brook, NY 11794, USA
[2]Department of Biological Sciences, Smith College, Northampton, MA 01063, USA
[3]Department of Migration, Max-Planck Institute for Animal Behavior, Radolfzell 78315, Germany
[4]Centre for the Advanced Study of Collective Behavior, University of Konstanz, Konstanz 78464, Germany
[5]Departament de Biologia Celular, Fisiologia i Immunologia, Universitat Autònoma de Barcelona, Cerdanyola del Vallès 08193, Spain
[6]Genome Integrity and Instability Group, Institut de Biotecnologia i Biomedicina, Universitat Autònoma de Barcelona, Cerdanyola del Vallès 08193, Spain
[7]Department of Integrative Biology, University of California, Berkeley, Berkeley, CA 94720, USA
[8]School of Biosciences, University of Kent, Canterbury, NJ, UK
[9]The Vertebrate Genomes Lab, Rockefeller University, New York, NY 10065, USA
[10]Tree of Life, Wellcome Sanger Institute, Hinxton, Cambridge CB10 1SA, UK
[11]Department of Biological Sciences, Texas Tech University, Lubbock, TX 79409, USA
[12]Department of Diagnostic and Interventional Radiology, University Medical Center Freiburg, Faculty of Medicine, University of Freiburg, Freiburg 79211, Germany
[13]Health Science and Technology, Aalborg University, Aalborg 9100, Denmark
[14]Department of Science, John Jay College of Criminal Justice, New York, NY 10019, USA
[15]Howard Hughes Medical Institute, Chevy Chase, MD 20815, USA
[16]Consortium for Inter-Disciplinary Environmental Research and Institute for Advanced Computational Science, Stony Brook University, Stony Brook, NY 11794, USA
[†]Lead author
*Corresponding authors. E-mails: wrthomas315@gmail.com; liliana.davalos@stonybrook.edu.
Associate editor: Bing Su

Abstract

***Sorex araneus*, the Eurasian common shrew, has seasonal brain size plasticity (Dehnel's phenomenon) and many intraspecific chromosomal rearrangements. Genomic contributions to these traits, however, remain unknown. We couple a chromosome-scale genome assembly with seasonal brain transcriptomes to discover relationships between molecular evolution and both traits. While Positively Selected Genes (PSGs) enriched the Fanconi anemia DNA repair pathway (*FANCI*, *FAAP100*), which is likely involved in chromosomal rearrangements by preventing the accumulation of chromosomal aberrations, genes under positive selection or showing seasonal differential expression in the brain implicate neurogenesis (*PCDHA6*, *SOX9*, Notch signaling) and metabolic regulation (*VEGFA*, *SPHK2*) as key mechanisms underlying Dehnel's phenomenon. We also find that both positively selected and differentially expressed genes in the hippocampus are overrepresented near *S. araneus* evolutionary breakpoints. This relates both positive selection and differential expression to accessible chromatin configuration, suggesting that chromosomal rearrangements are integral to adaptive evolution and the regulation of brain size plasticity.**

Keywords highly contiguous genome assembly, shrew, Dehnel's phenomenon, evolutionary breakpoints, chromosomal evolution, cortex, hippocampus

Received: June 17, 2025. **Revised:** November 11, 2025. **Accepted:** December 19, 2025

Introduction

Sorex araneus, the Eurasian common shrew, exhibits two rare and remarkable phenotypes: extensive intraspecific chromosomal rearrangements (Searle et al. 2019) and Dehnel's phenomenon or seasonal size plasticity (Dehnel 1949; Pucek 1965; Lázaro et al. 2018a; Lázaro and Dechmann 2021). While chromosomal rearrangements are common across species boundaries, populations of *S. araneus* have extensive karyotypic diversity within species, forming distinct chromosomal races (Searle et al. 2019). This shrew also undergoes dramatic, reversible changes in size, including of the brain, in response to seasonal environmental shifts (Dehnel 1949; Pucek 1965; Lázaro et al. 2018a; Lázaro and Dechmann 2021), and is one of the few mammals known to deploy this wintering strategy (Lapoint et al. 2017; Ray et al. 2020; Nováková et al. 2022). *S. araneus* reach an initial size maximum as juveniles in their first summer, followed by shrinking of most organs in the autumn in response to decreased temperatures (Lázaro et al. 2019). Size change also occurs in the brain, with the largest absolute decrease in the cortex (Lázaro et al. 2018a). Size reaches a minimum in winter, with rapid regrowth to a second size maximum the following spring (Dehnel 1949; Pucek 1965; Lázaro and Dechmann 2021), simultaneous with pubescence for the single breeding season of their disproportionately short lifespan (Healy et al. 2014). Research on the genomic basis of these traits is, however, very recent and has been limited to gene expression analyses (Thomas et al. 2025, 2026).

Previous cellular and molecular investigations of Dehnel's phenomenon in *S. araneus* have discovered that seasonal brain size change occurs without a reduction in neuronal number (Baldoni et al. 2025b), suggesting the evolution of neuroprotective mechanisms. Seasonal gene expression analyses of the *S. araneus* hypothalamus showed enrichment of upregulated genes involved in apoptosis regulation and cancer pathways during autumn brain shrinkage, highlighting a balance between cell proliferation and death (Thomas et al. 2025). While the antiapoptotic gene *BCL2L1* was upregulated during shrinkage, *SPHK2*, which promotes apoptosis (Liu et al. 2003; Maceyka et al. 2005) and increases activity in the brains of patients with Alzheimer's disease (Takasugi et al. 2011), was evolutionarily upregulated compared to other mammals. Those findings highligthed a finely tuned system that enables common shrews to reversibly regulate brain shrinkage while avoiding the detrimental effects typically associated with neurodegeneration.

Despite those insights, the molecular evolutionary processes involved in the traits that make *S. araneus* unique, extensive chromosomal rearrangements and Dehnel's phenomenon, remain unknown. While intraspecific karyotypic diversity in mammals is not uncommon (White et al. 2010; Ruiz-Herrera et al. 2012; Benathar et al. 2019), the more than 75 distinct chromosomal races in *S. araneus* indicate unique chromosomal instability (Searle et al. 2019). Similarly, Dehnel's phenomenon, though most pronounced in the common shrew, is exceptionally rare among mammals, found only in some red-toothed shrews (Soricinae) (Lázaro and Dechmann 2021), the European mole (*Talpa europaea*) (Nováková et al. 2022), and two mustelid species (*Mustela erminea*, *Mustela nivalis*) (Lapoint et al. 2017). A similar phenotype is also found in the domesticated ferret (*Mustela putorius furo*) (Apfelbach and Kruska 1979) and the pygmy shrew (*S. etruscus*) (Ray et al. 2020), which diverged from *Sorex* ~20 mya (Dubey et al. 2007). Dehnel's phenomenon is rare, as is the genomic instability of *S. araneus*. While the former must be associated with positive selection to adapt to the ecophysiological challenges these species face, the latter could result from relaxed negative selection on genome repair mechanisms.

Dehnel's phenomenon is hypothesized to have evolved as an adaptive tradeoff between size and metabolic demand during winter (Lázaro and Dechmann 2021), highlighted by the size response to temperature (Lázaro et al. 2019). This strategy is critical for the common shrew, which has one of the highest mammalian basal metabolic rates per unit of body mass (Ochocińska and Taylor 2005). By reducing the size of energy expensive tissues, shrews decrease the energy required for their maintenance and movement (Pucek 1965, 1970; Hyvärinen 1984; Churchfield et al. 2012; Taylor et al. 2013; Keicher et al. 2017; Lázaro et al. 2019; Schaeffer et al. 2020; Thomas et al. 2026). Recent evidence on the metabolic and gene expression changes concurrent with seasonal size change in the common shrew has lent support to this hypothesis (Thomas et al. 2026). For example, blood metabolomics and liver transcriptomics indicate increased lipid metabolism and gluconeogenesis during shrinkage (Thomas et al. 2026). These may be regulated by adaptive gene expression of the hypothalamus blood–brain barrier (Thomas et al. 2025). The evolution of efficient metabolic regulation systems is therefore expected during seasonal size change.

A new chromosome-level genome assembly for the common shrew provides an opportunity to investigate how selection has shaped both the convergently evolved Dehnel-like phenotypes and the unique chromosomal instability of these shrews. We compared *S. araneus* chromosome rearrangements to closely related species, applied branch-site models to identify *S. araneus*-specific and Dehnel-associated positively selected genes (PSGs), and integrated results with seasonal gene expression data from the common shrew cortex and hippocampus. We discovered gene enrichment of *S. araneus*-specific PSGs in the Fanconi anemia pathway (*FANCI*, *FAAP100*, *PALB2*), associated with DNA repair and longevity, as well as in *VEGFA*, a candidate hypothalamic regulator of metabolism in the common shrew. Genes associated with neurogenesis (*PCDHA6*, *SOX9*) also showed signatures of parallel evolution across species with Dehnel's phenomenon, complementing the seasonal changes identified in the hippocampus and cortex linked to cell proliferation (*SOX9*) and Notch signaling. Together, these integrated genomic and expression analyses implicate changes in genes involved in metabolism and cell proliferation in the evolution of Dehnel's phenomenon while also characterizing evolutionary processes associated with chromosomal rearrangements and *S. araneus* adaptation.

Results

Genome assembly, annotation, and synteny

We sequenced, assembled, and annotated a chromosome-scale reference genome assembly for one female Eurasian common shrew, *S. araneus*, following the Vertebrate Genomes Project (VGP) assembly pipeline (Rhie et al. 2021) using a combination of Illumina short-read, PacBio long-read, and Hi-C sequencing.

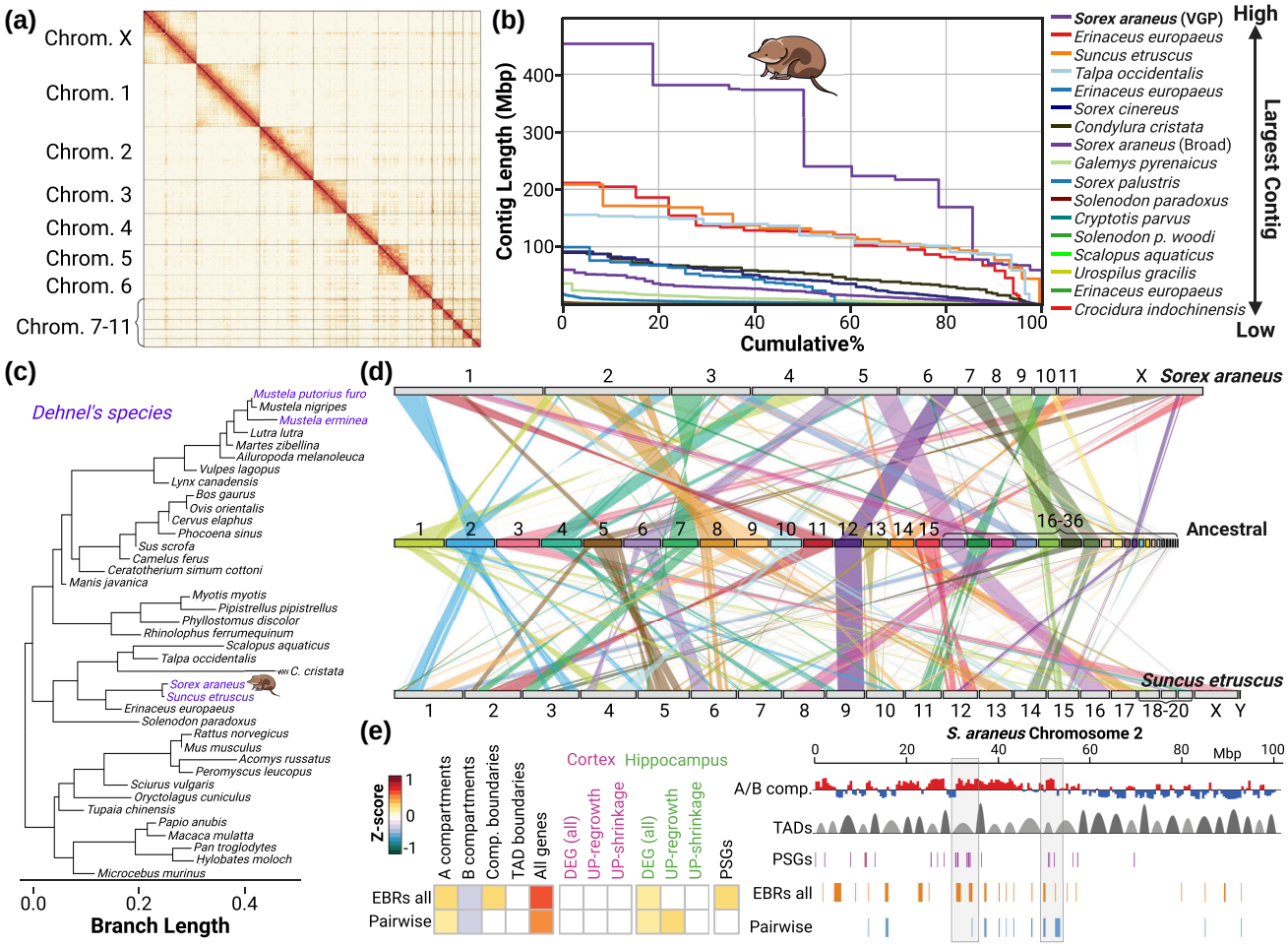

Figure 1 Genome assembly and comparisons. a) Using PacBio and Hi-C chromosome interactions and manual curation, the shrew genome assembly was assembled into 12 chromosomes. b) Cumulative percent of each Eulipotyphla genome found on contigs of certain length, showing a highly contiguous shrew genome assembly and longer chromosomes than those of other close relatives. c) Phylogeny of species used in comparative genomic analyses, each with more than 16,000 genes and BUSCO scores greater than 80%. d) Syntenic comparisons between *S. araneus*, the Eulipotyphla ancestor, and *S. etruscus* orthologous blocks highlighting chromosome fissions and fusions. e) Multicomparison heatmaps showing pairwise correlations between EBRs and various genomic features including compartments (a and b), TAD boundaries, and DEG in the cortex and hippocampus. The panel on the right represents a zoomed-in view of chromosome 2–specific tracks showing A/B compartments, TAD distribution, PSGs, and EBRs.

PacBio sequencing data had 35.71× genome coverage with a genome size of ∼2.40 Gb. We used Hi-C chromosomal interactions to further manually curate the genome and were able to anchor >99.8% of the genome to 12 chromosomes (2N = 24) (Fig. 1a) with a scaffold N50 of 374 MB (Fig. 1b) and an estimated a genome size of ∼2.23 Gb consisting of 73% unique or nonrepetitive sequence. By comparison, the previous *S. araneus* genome assembly from the Broad Institute consisted of 12,845 unplaced scaffolds (Table 1; Fig. 1b). Annotations using the Tool to infer Orthologs from Genome Alignments's (TOGA) machine learning ortholog classifier identified 42,221 transcripts associated with 17,246 genes (Benchmarking Universal Single-Copy Orthologs [BUSCO] mammalia_odb10; 9,005 complete genes; 97.6%), of which 15,980 were one-to-one orthologs to the human genome (Fig. S1). These numbers are similar to those identified with RNA sequencing, which found 45,362 transcripts associated with 24,205 coding loci, of which 15,752 are annotated genes.

Pairwise alignments between *S. araneus* and other species of the order Eulipotyphla with high-quality genome assemblies showed conserved syntenic regions between species. Comparing the Eurasian common shrew to its closest relative in the dataset, the pygmy shrew *Suncus etruscus*, we found 236 orthologous blocks (Fig. 1d). These blocks show that *S. araneus* chromosome 10 is orthologous to *S. etruscus* chromosome 11, and *S. araneus* chromosome 11 is orthologous to *S. etruscus* chromosome 17. Pairwise comparisons also show that large portions of *S. araneus* chromosome 7 are syntenic with *S. etruscus* 3, and *S. araneus* 8 with *S. etruscus* 14, while *S. araneus* chromosome X appears to be fusions of *S. etruscus* X, 5, and 12, with *S. araneus* chromosome 5 being fusions of *S. etruscus* 6, 9, and 16. Meanwhile, *S. araneus* chromosomes 2, 3, and 4 show extensive rearrangements compared to *S. etruscus*.

We also inferred that the ancestor of Eulipotyphla (atE) had 36 chromosomes (2N = 72) using DESCHRAMBLER (Kim et al. 2017). This reflects a drastic reduction in chromosome number between the atE and Soricidae. Despite this reduction, many chromosomes retain clear one-to-one orthology with those of the pygmy shrew (*S. etruscus*) and the atE, indicating strong conservation of

Table 1 Chromosome quality of the new *S. araneus* genome assembly compared to the Broad Institute assembly.

	Broad Institute (sorAra2)	New assembly (mSorAra2.pri)
Total sequence length	2,423,158,183	2,405,993,548
Total ungapped length	2,192,103,426	2,393,049,584
Number of scaffolds	12,845	65
Scaffold N50	22,794,405	374,364,821
Scaffold L50	36	3
Number of contigs	201,420	1,492
Contig N50	22,623	4,024,507
Contig L50	27,135	182
Chromosomes	0	12
Source location	Piel Island, United Kingdom	Radolfzell, Germany

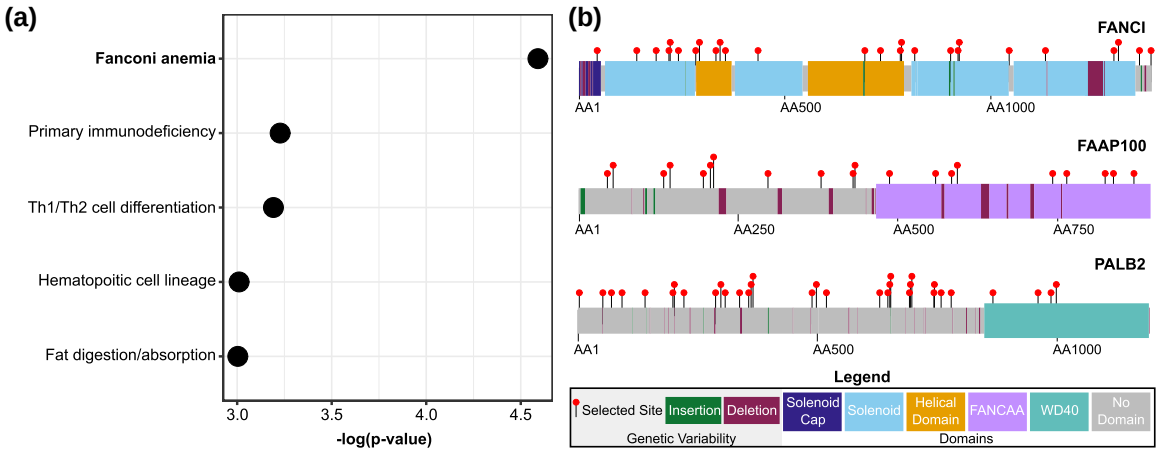

Figure 2 Gene set enrichment of shrew-specific PSGs. a) Five pathways were significantly enriched ($P < 0.05$) with PSGs only under selection in the *S. araneus* lineage. The most enriched pathway was the Fanconi anemia complex, consisting of b) *FANCI*, *FAAP100*, and *PALB2*, with >19 positively selected sites per gene detected from MEME. Genetic variability (selected amino acids, insertions, deletions) was found across genes, both within and between protein domains.

macroscale synteny. For example, pairwise comparisons (Fig. 1d) reveal that several of the smaller chromosomes remain largely unchanged between *S. araneus* and the atE (*S. araneus* C7 ≅ atE C21, *S. araneus* C8 ≅ atE C22, *S. araneus* C9 ≅ atE C20, *S. araneus* C10 ≅ atE C17, *S. araneus* C11 ≅ atE C14) (Data S1). Lastly, the reconstruction of ancestral genomes allowed us to identify 574 Evolutionary Breakpoint Regions or EBRs across *S. araneus*, *S. etruscus*, *Galemys pyrenaicus, Talpa occidentalis*, *Condylura cristata*, *Erinaceus europaeus*, *Phyllostomus discolor*, and *Rhinolophus ferrumequinum* and 224 EBRs between *S. araneus* and *S. etruscus.*

Positive selection in *S. araneus*

We then analyzed the molecular evolution between the common shrew and other mammal species (Fig. 1c; Data S2) by testing for positive selection in more than 15,000 single-copy orthologs using adaptive branch-site random effects likelihood (aBSREL) models implemented in the HyPhy suite (v2.5.32) (Kosakovsky Pond et al. 2020). We detected evidence of positive selection in 676 genes (PSGs; $P_{adj} < 0.05$) in *S. araneus* (Fig. 2a; Data S3). Gene set enrichment analysis identified eight Kyoto Encyclopedia of Genes and Genomes (KEGG) pathways enriched by *S. araneus* PSGs, consisting of four related to immunity, including complement and coagulation cascades (4.1-fold enrichment, $P < 0.01$), hematopoietic cell lineage (3.1-fold enrichment, $P < 0.05$), primary immunodeficiency (5.1-fold enrichment, $P < 0.05$), and inflammatory bowel disease (3.6-fold enrichment, $P < 0.05$). Additionally, the Fanconi anemia pathway, associated with genomic stability, was enriched (4.3-fold enrichment, $P < 0.05$), including genes *FANCI* (Fig. 2b), *PALB2*, *FAAP100*, and *REV3L*.

Exploratory analyses on background branches inferred 2,997 genes to be evolving under positive selection in at least one background species, of which 288 genes showed signals of pervasive selection throughout the phylogeny (>5 background species). Of the 676 *S. araneus* PSGs, 231 genes showed no signal of background selection and were thus specific to this species (Data S4). KEGG gene set enrichment of the 231 *S. araneus*-specific PSGs also identified an enrichment of the Fanconi anemia pathway (8.7-fold enrichment, $P < 0.05$), hematopoietic cell lineage (4.8-fold enrichment, $P < 0.05$), and primary immunodeficiency (9.3-fold enrichment, $P < 0.05$), as well as Th1 and Th2 cell differentiation (5.1-fold enrichment, $P < 0.05$) and fat digestion and absorption (8.3-fold enrichment, $P < 0.05$).

Table 2 Counts of genes tested and found to be under positive selection by species

Species	Total genes	Count including this tip	Species specific	Convergent (shrew + 2)	Convergent (<5 background)	Convergent (<1 background)
S. araneus	15,812	676	231	23	8	1
S. etruscus	15,380	904	397	19	6	0
M. erminea	16,675	225	54	21	6	1
M. putorius furo	16,638	110	40	7	4	1

For all counts statistical significance at $P_{adj} < 0.05$.

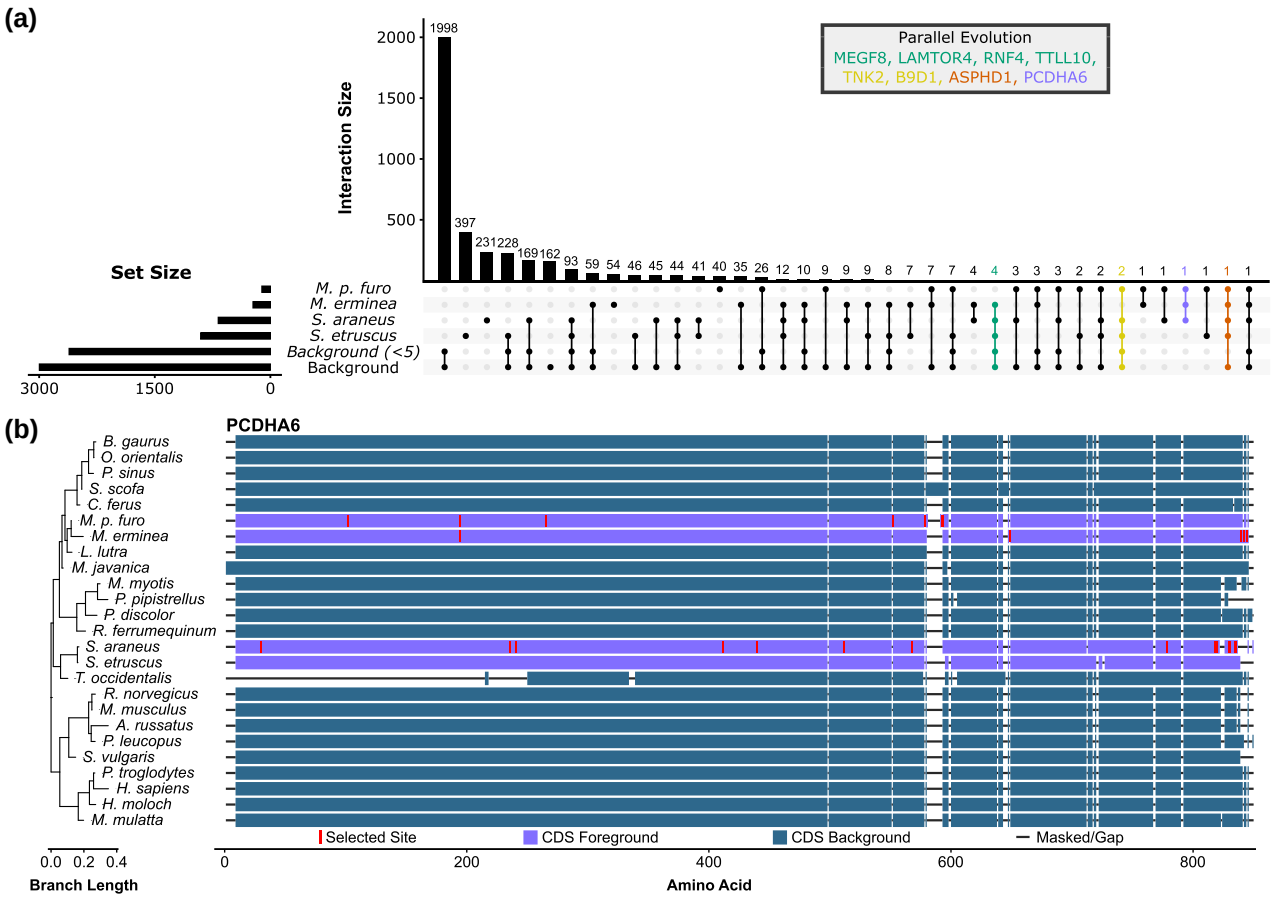

Figure 3 Signatures of parallel evolution in Dehnel's phenomenon. a) Upset plot of the PSGs found in *S. araneus*, species with Dehnel-like phenotypes, and background branches with two degrees of stringency (background selection > 0 and background selection > 4). Eight genes overlapped across species with Dehnel-like traits were found. b) The gene encoding protocadherin alpha 6, *PCDHA6*, was the single gene convergently evolving under positive selection in *S. araneus*, *M. erminea*, and *M. putorius furo* without background selection.

Parallel evolution of Dehnel's phenomenon

We tested for selection in more than 10,000 genes annotated in all the selected mammal species with Dehnel-like phenotypes (*M. erminea*, *M. putorius furo*, *S. etruscus*) and inferred positive selection in over 100 genes per species, with various degrees of parallel evolution between species. We inferred 225 genes to be under positive selection ($P_{adj} < 0.05$) in *M. erminea*, 110 genes in *M. putorius furo*, and 904 genes in *S. etruscus* (Table 2). Accounting for background selection, eight genes show signatures of parallel evolution with only episodic (<5 species) background selection (*ASPHD1*, *PCDHA6*, *TNK2*, *B9D1*, *MEGF8*, *TTLL10*, *RNF34*, *LAMTOR4*), significantly more genes than expected by chance (100,000 permutations, $P < 0.0001$), suggesting nonindependence with lineage-specific traits, ie Dehnel's phenomenon (Fig. 3). A single gene, *PCDHA6*, was parallel between *S. araneus*, *M. erminea*, and *M. putorius furo* with no background

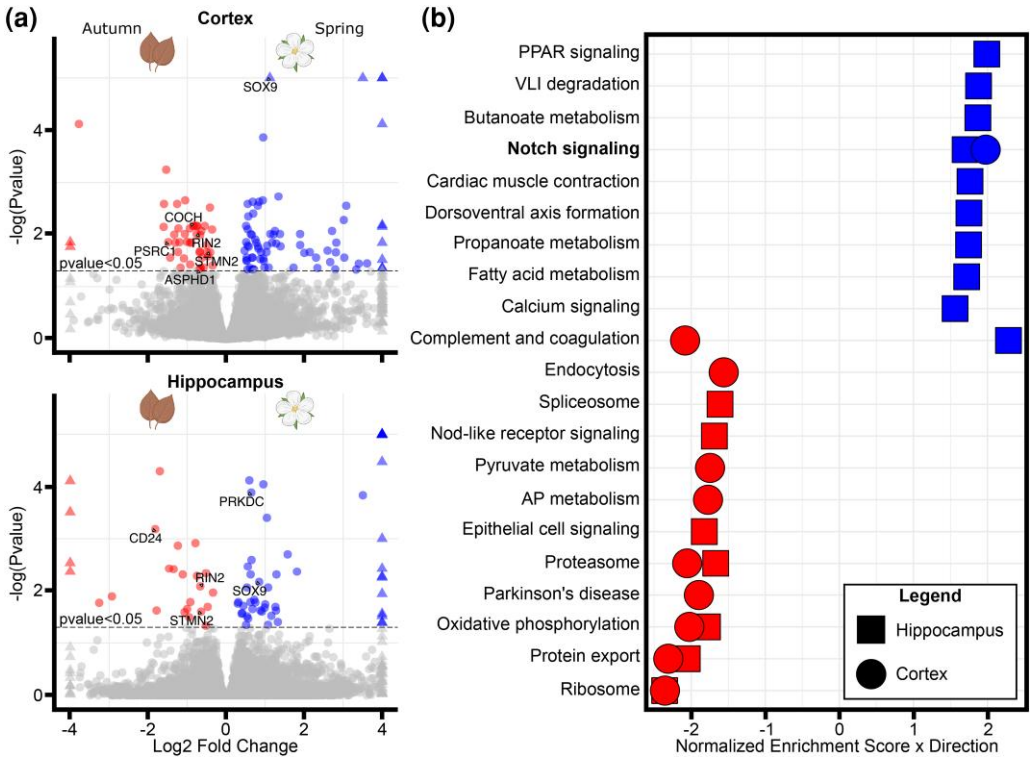

Figure 4 Seasonal gene expression of the hippocampus and cortex. a) Volcano plot of DEGs in the cortex and the hippocampus between autumn (left; cortex, 46 upregulated genes; hippocampus, 25 upregulated genes) and spring (right; cortex, 76 upregulated genes, hippocampus, 52 upregulated genes). b) Gene set enrichment of DEGs identified 21 total enriched gene sets ($P_{adj} < 0.05$), five of which overlap in the same direction between the two brain regions (Notch signaling, proteasome, oxidative phosphorylation, protein export, ribosome).

selection. Mixed effects model of evolution (MEME) analyses were used to detect specific sites evolving under positive selection on *S. araneus* PSGs and found several sites to be convergent across species with Dehnel-like phenotypes. Across the eight genes inferred to be under parallel evolution, ten sites were found to have positive selection in multiple species with Dehnel-like phenotypes.

Seasonal brain expression

To explore both the regulatory mechanisms of seasonal brain size change and relationships between molecular evolution and function, we tested for differential expression between the shrinking (autumn) and regrowth (spring) phases of Dehnel's phenomenon in two brain regions (Data S5), the hippocampus and the cortex, and identified any overlapping PSGs. In the hippocampus, we found 77 differentially expressed genes (DEGs) between autumn and spring, with 52 significantly upregulated in spring and 25 significantly upregulated in autumn (Fig. 4; Data S6). Using a ranked gene set enrichment analysis, we discovered an enrichment of 17 pathways (seven upregulated in autumn, ten upregulated in spring), which included many pathways associated with metabolism: peroxisome proliferator-activated receptor or PPAR signaling ($P_{adj} < 0.01$, normalized enrichment score or NES = 1.81), fatty acid metabolism ($P_{adj} < 0.01$, NES = 1.81), and oxidative phosphorylation ($P_{adj} < 0.01$, NES = 1.81) (Fig. 4b). In the cortex, we identified 122 significant DEGs, with 46 upregulated in autumn shrinkage and 76 upregulated in spring regrowth. Ten pathways were enriched with genes varying between these seasons, including five that overlapped in the same direction with those enriched in the hippocampus: ribosome (cortex: $P_{adj} < 0.001$, NES = −2.35; hippocampus: $P_{adj} < 0.001$, NES = −2.36), protein export (cortex: $P_{adj} < 0.001$, NES = −2.31; hippocampus: $P_{adj} < 0.01$, NES = −2.05), oxidative phosphorylation (cortex: $P_{adj} < 0.001$, NES = −2.02; hippocampus: $P_{adj} < 0.01$, NES = −1.78), proteasome (cortex: $P_{adj} < 0.01$, NES = −2.05; hippocampus: $P_{adj} < 0.05$, NES = −1.67), and Notch signaling (cortex: $P_{adj} < 0.01$, NES = 1.98; hippocampus: $P_{adj} < 0.05$, NES = 1.70). Of the DEGs, six genes in the cortex and five genes in the hippocampus overlapped with PSGs, three of which were found in all three datasets (*SOX9*, *RIN2*, *STMN2*) (Fig. 5).

Hypothalamus expression overlap

There were many instances of overlap between PSGs and prior results. Previous analyses identifying DEGs in the hypothalamus between seasons of Dehnel's phenomenon (Thomas et al. 2025) only consisted of six overlapping genes with PSGs (*KCNK12*, *COCH*, *RSPH3*, *KNDC1*, *PARP4*, *FAN1*). However, comparing PSGs to previous work identifying branch specific change in hypothalamus expression in *S. araneus* (Fig. 5), we found overlap in genes related to hypothalamus development. Eleven PSGs (*KIAA0930*, *LOXL1*, *MLST8*, *PIGR*, *VEGFA*, *GALNT12*, *POLDIP3*, *NXPH3*, *SPHK2*, *GRIP2*, *FANCI*) overlapped with those having higher expression in the *S. araneus* hypothalamus compared to other mammalian species. *VEGFA* was found in this overlap, which we hypothesized was important for

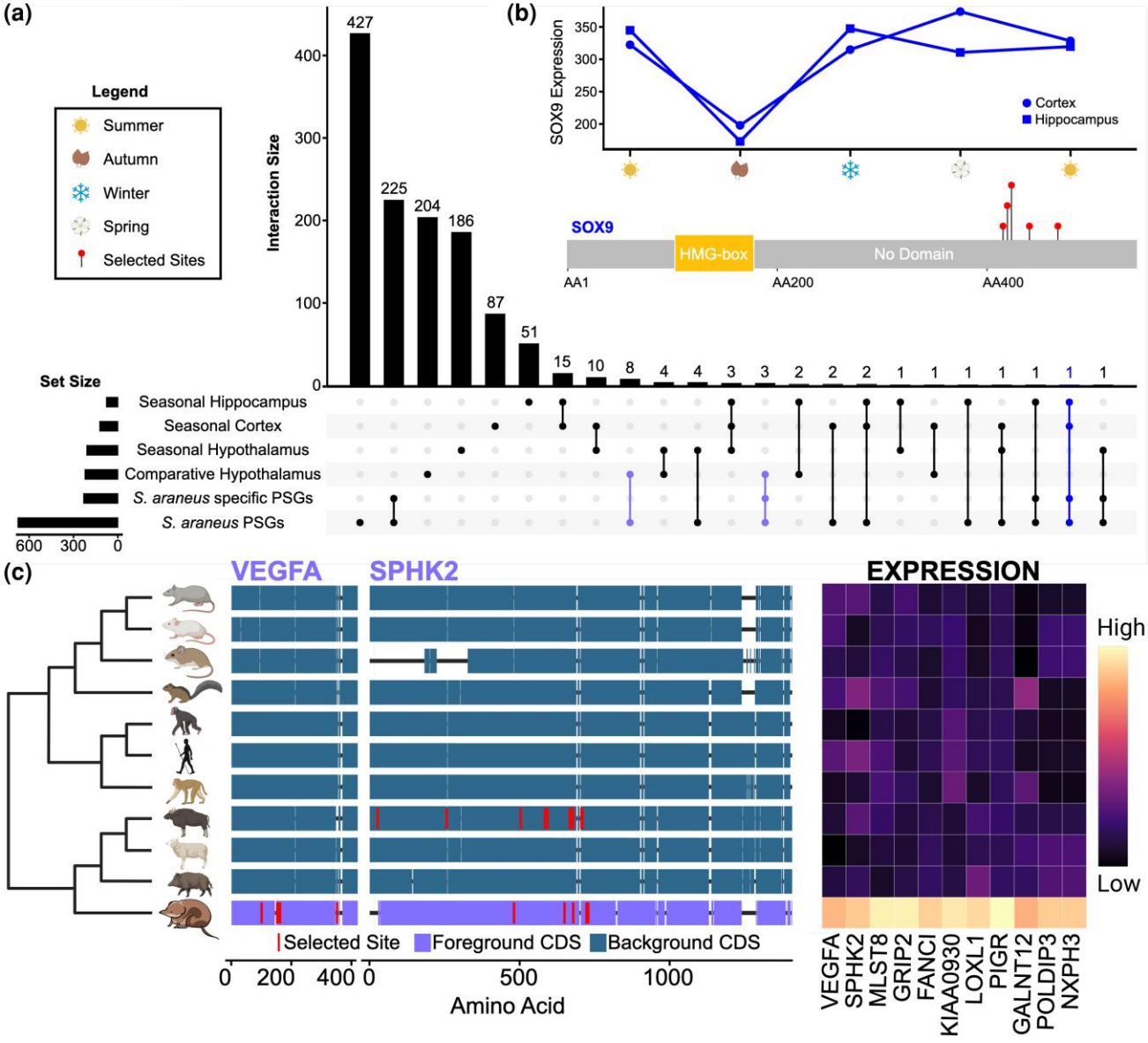

Figure 5 Evolutionary and seasonal expression divergence in the brain associated with positive selection in coding sequence. a) Upset plot of the PSGs found in *S. araneus* compared to significantly varying genes from transcriptomics analyses. b) SOX9, involved in neural stem cell maintenance, is the only gene both downregulated in the hippocampus and cortex during brain shrinkage and has positively selected changes in its coding sequence outside of a known domain. c) Positive selection was also identified in *VEGFA*, involved in blood–brain barrier development and function, and *SPHK2*, which regulates neuronal cell death. Both genes are part of a suite of 11 PSGs with upregulated expression in *S. araneus* hypothalamus compared to other mammals.

S. araneus hypothalamus fenestration to improve signaling of metabolic demands across the blood–brain barrier. Of the eight overlapping genes, three were *S. araneus*-specific, *LOXL1*, *GALNT12* and *FANCI*. Overlap between PSGs and expression data may indicate selection in coding sequence to alter gene function and regulation.

Evolutionary genome instability correlates with PSGs in open chromatin domains

Previous studies have suggested that lineage-specific evolutionary genomic reshuffling can be integral to adaptive evolution, influencing gene expression, chromatin architecture, and phenotype–environment interactions (Crombach and Hogeweg 2007; Álvarez-González et al. 2022a). To investigate this in *S. araneus*, we examined higher-order chromatin organization and its relationship with EBRs and PSGs. Using Hi-C data, we characterized the 3D genome structure, identifying A/B compartments and topologically associating domains (TADs). The genome-wide distribution of A/B compartments was consistent with patterns observed in other mammals (Álvarez-González et al. 2022b), with 48.8% of the genome assigned to A compartments, indicative of open chromatin.

Importantly, EBRs were significantly enriched within accessible A compartments (permutation test based on 10,000 permutations, normalized z-score = 0.226, $P = 0.005$) and genes (normalized z-score = 0.585, $P = 0.0002$) (Fig. 1e; Fig. S2).

Notably, both DEGs detected in the hippocampus (z-score = 0.211, $P = 0.021$) and PSGs were significantly enriched at EBRs (z-score = 0.275, $P = 0.0004$) (Data S7), statistically linking chromatin architecture, gene regulation, and evolutionary adaptation in *S. araneus*.

Discussion

S. araneus chromosomal evolution

The size and positioning of syntenic regions between *S. araneus*, *S. etruscus*, and the ancestral Eulipotyphla (atE) chromosomes provides insight into past processes of chromosome evolution (Fig. 1). The reduced number of chromosomes since the atE and the conservation of smaller chromosomes suggest that extensive chromosomal fusions have occurred since the atE in larger chromosomes, particularly within the ∼20 million years since the most recent common ancestor (MRCA) of *Sorex* and *Suncus* (Dubey et al. 2007). In total, we infer 29 fusion events and 5 fissions, with many fusions involving large chromosomes (eg *S. araneus* C1 and C2) (Data S7). A particularly notable case is the X chromosome: while the ancestral mammalian X is conserved (atE C3, *S. etruscus* CX), it has undergone a tandem fusion with autosomes (atE C5/*S. etruscus* C5 and atE C15/*S. etruscus* C12). This fusion validates previous cytogenetic work for the *S. araneus* X chromosome (Sharman 1956), highlighting not only the accuracy of our assembly but also its utility for inferring chromosome evolution in Eulipotyphla.

Despite recovering clear fusion events, many complex rearrangements remain unresolved, with ∼30 syntenic regions that cannot be confidently classified as fissions or fusions with these data. These ambiguities may reflect the highly dynamic chromosomal evolution of *S. araneus*, a species renowned for its karyotypic instability (Searle et al. 2019). For example, based on chromosome number and geography, the closest land races with 11 autosomes are the Cordon and Pelister groups (Searle et al. 2019), yet these populations are ∼400 and 1,800 km from the German population, highlighting dynamic intraspecific changes and potentially adding to the more than 75 already documented chromosomal races in this species.

Although extraordinary, *S. araneus* is not alone in exhibiting rapid karyotypic turnover. High rates of chromosomal change have evolved in specific groups, such as Cetartiodactyla, and within specifies, as seen in brocket deer species (*Mazama* sp.) (Galindo et al. 2021), lemurs (*Eulemur* sp.) (Searle and Hughes 2025), arctic foxes (*Alopex lagopus*) (MØller et al. 1985), bats (eg phyllostomids) (Gomes et al. 2012), bovids (Bruère 1975; Troshina et al. 1985), and numerous rodents (Yosida 1976; Bardhan and Sharma 2000; Romanenko et al. 2019). The only clear rival to *S. araneus* in terms of chromosomal race diversity is the house mouse (*Mus musculus domesticus*), which has evolved over 100 Robertsonian chromosomal races (Garagna et al. 2014), with drastic effects on the genomic landscape and gene regulation (Vara et al. 2021; Marín-García et al. 2024). Building on our findings, future analyses resolving chromosomal relationships of *S. araneus* both within species and across all mammals will provide a powerful framework for identifying the regulatory and evolutionary mechanisms that drive extreme karyotypic diversity.

Neuronal proliferation, metabolism, and Dehnel's phenomenon

Distinct molecular changes likely underlie the evolution of Dehnel's phenomenon, as molecular parallelism associated with these phenotypes was rare. Tests for parallel molecular evolution uncovered eight genes overlapping across species with Dehnel-like traits (Fig. 3), significantly more than expected by chance ($P < 0.0001$). Consistent with an association with extraordinary brain size plasticity, the gene encoding protocadherin alpha 6, *PCDHA6*, is the only one to show signatures of parallel positive selection across species with Dehnel-like phenotypes without background selection. PCDHA6 is part of the protocadherin alpha cluster, a group of cell adhesion molecules central to brain organization, neuronal circuity, axon maintenance, and synaptic plasticity (Yagi and Takeichi 2000; Fukuda et al. 2023). While in mice *PCDHA* knockout leads to miswiring of hippocampal connectivity despite normal neurogenesis (Chen et al. 2017), in cell lines, *PCDHA6* knockout results in altered neurite morphology (Vadodaria et al. 2019). Indicating functional conservation, there was high sequence conservation in species in which this gene was present (though 15 of 40 assemblies lost or missed the gene). Substitutions in *S. araneus*, *M. erminea*, and *M. putorius furo* may contribute to maintain, rewire, or regenerate synapses during seasonal changes in brain size and morphology, but *PCDHA6* was not detected in brain expression, weakening the case for its genetic contribution to brain size plasticity. This dearth of parallel PSGs without background selection in Dehnel-like phenotypes makes the common shrew a unique model for researching brain size plasticity.

As comparative tests for convergent evolution did not identify strong candidate genes associated with Dehnel's phenomenon across species, we focused on *S. araneus*-specific PSGs and analyzed gene expression, both seasonally variable and evolutionarily upregulated (previously published in (Thomas et al. 2025)). To the best of our knowledge there is no prior study of sequence and expression patterns with the massive changes seen in Dehnel's phenomenon, so the question of how sequence and expression evolve provides crucial context for our results. First, genes expressed in the brain diverge less in their sequences than those expressed in other tissues (Khaitovich et al. 2005). Second, expression divergence in the brain is also diminished compared to other tissues (Lemos et al. 2005b). Third, although the rate of nonsynonymous substitutions sometimes correlates with expression divergence (Lemos et al. 2005a) (eg in *Drosophila* (Nuzhdin et al. 2004)), this is not always the case especially when analyzed between species (eg in birds (Dean et al. 2015)). In short, divergence in either sequence or expression of brain-expressed genes is rare, and the two types of change may or may not be correlated.

Despite the expectation of strongly conserved brain gene expression (Khaitovich et al. 2006), including throughout development (Cardoso-Moreira et al. 2019; Sepp et al. 2024), we identified seasonal expression plasticity in pathways related to cellular proliferation, differentiation, and death. Previously, expression analyses of the *S. araneus* hypothalamus indicated anti-apoptotic pathways, mediated by *BCL2L1* and *NFKBIA*, are upregulated in autumn (Thomas et al. 2025). That suggested

the common shrew brain actively regulates pathways to avoid cell loss, consistent with the constant or increasing number of neural cells during brain shrinkage (Baldoni et al. 2025b). But we did not observe upregulation of those pathways in the hippocampus or cortex during autumn. Instead, we identified significant changes in Notch signaling in both regions. In *S. araneus*, Notch signaling was under-expressed during brain shrinkage (Fig. 4). Notch signaling is a highly conserved pathway in animals, well characterized for its role in development (Artavanis-Tsakonas et al. 1999) and a master regulator of plasticity in the adult brain of model organisms (Yoon and Gaiano 2005; Ables et al. 2011).

In the *S. araneus* hippocampus and cortex, we found autumn changes in gene expression consistent with enhanced neurogenesis. While the precise effects of the Notch signaling decrease are unknown, decreased Notch can promote neural stem cell proliferation and increased adult neurogenesis (Chapouton et al. 2010), depleting stem cell populations and hindering neuronal migration (Hashimoto-Torii et al. 2008). In spring, *S. araneus* revert to elevated expression of *NOTCH1*, which can decrease the rate of neuron establishment between winter and summer in the hippocampus and cortex (Baldoni et al. 2025b). Notch signaling also regulates *SOX9* expression, which is critical for maintaining neural stem cells (Scott et al. 2010; Vong et al. 2015), with *SOX9* knockdown in mice leading to increased neurogenesis (Cheng et al. 2009). As with Notch signaling, we observed decreased *SOX9* expression in the cortex and hippocampus of autumn, shrinking *S. araneus* (Figs. 4 and 5). Consistent with our interpretation of enhanced autumn neurogenesis, winter shrews increased neuron counts in the hippocampus and cortex compared to summer juveniles (Baldoni et al. 2025b). Despite being highly conserved among background species, as expected for a developmental and brain-expressed gene, *S. araneus SOX9* is also under positive selection (Fig. 5). Most disease-related genetic variation in *SOX9* is associated with developmental disorders, particularly chondrogenesis (cellular bone proliferation) and sex determination (Kwok et al. 1995; Pritchett et al. 2011; Csukasi et al. 2019); however, coding changes could alter the function of this gene in hitherto unsuspected *S. araneus*-specific neurogenic processes.

PSGs related to both metabolic regulation and cell proliferation (n = 11) also overlapped with genes evolutionarily upregulated in the *S. araneus* hypothalamus, supporting the hypothesis that Dehnel's phenomenon evolved as metabolic adaptation. *VEGFA* and *SPHK2* were under positive selection in *S. araneus* while also showing an approximate 4-fold upregulation in the *S. araneus* hypothalamus compared to other mammals (Fig. 5) (Thomas et al. 2025). Upregulation of *VEGFA* can increase blood–brain barrier permeability, improving nutrient sensing in the brain, while upregulation of *SPHK2* may be involved with neuronal cell death, as overexpression of *SPHK2* in stressed mice cells promotes apoptosis (Liu et al. 2003; Maceyka et al. 2005). Positively selected substitutions may benefit the common shrew. For example, we propose that substitutions in *VEGFA* can alter blood–brain barrier vascularization in *S. araneus*, as different isoforms can be pro- or antiangiogenic (Küsters et al. 2003; Arcondéguy et al. 2013), while substitutions in *SPHK2* may reduce the apoptotic effect of this gene in the brain, allowing evolutionary overexpression of each in the *S. araneus* hypothalamus.

Selection on DNA repair, associations with longevity, and impacts on chromosomal variation

In *S. araneus*, positive selection enriched genes in the Fanconi anemia pathway, which may be associated with reduced shrew longevity and chromosomal instability. We found evidence of positive selection in *FANCI*, whose encoded protein heterodimerizes with FANCD2 to form an ID complex that localizes to chromatin in response to damage (Smogorzewska et al. 2007; Alcón et al. 2020; Alcón et al. 2024). We also identified several PSGs related to the FANCI–FANCD2 DNA repair complex: *FAAP100*, which is required for core complex stability with knockouts leading to FA-mediated genomic instability (Ling et al. 2007), and *PALB2*, whose involvement in the PALB2–BRCA2 complex promotes chromatin stability and homologous recombination DNA repair pathways (Xia et al. 2006; Guo et al. 2015). While amino acids within protein-binding domains are generally more conserved than those in other regions (FAAP100–FANCA domain = 2.0 vs. 2.6 in nondomain regions; PALB2–WD40 domain = 1.2 vs 3.4 substitutions per 100 amino acids), many positively selected sites fall within these domains, suggesting potential protein–protein interactions that may modulate DNA repair complex activity.

DNA damage responses and genomic stability are linked with lifespan evolution, as DNA must be constantly repaired throughout life to reduce the risk of cancer and other age-related diseases (Christensen et al. 2006; Debrabant et al. 2014; MacRae et al. 2015; Yousefzadeh et al. 2021). Impaired Fanconi anemia DNA repair pathways are mechanistically linked to premature aging (Brosh et al. 2017) and cancers (Reid et al. 2007; Xia et al. 2007). By contrast, strong positive selection in DNA repair mechanisms, including *FANCI*, has been found in parrots and other long-lived bird species (Wirthlin et al. 2018). Contrasting long-lived species, *S. araneus* have a lifespan half that predicted by their size (Healy et al. 2014), reducing the value of maintaining genomic stability. This would relax negative selection on DNA repair pathways and, in turn, co-opt them into alternative functions perhaps related to the propensity for chromosomal rearrangements. But this would also contribute to the short lifespan of *S. araneus*, as such modifications would expose older shrews to age-related diseases. Thus, substitutions for genes in this pathway in *S. araneus*, especially in protein domains, may impair or alter DNA repair and recombination processes and thus increase the generation of structural variation. As genetic variation provides the substrate for evolutionary change, these rearrangements could also further enhance subsequent local adaptation in this geographically widespread species. Supporting this view, a recent model has proposed an integrative framework linking evolutionary genome reshuffling with DNA damage response mechanisms and the dynamic spatial organization of germ cell genomes (Álvarez-González et al. 2022b).

Conversely, chromosomal rearrangements may not only arise as a consequence of selection on DNA repair but could shape adaptive evolution in *S. araneus*. We found an overrepresentation of PSGs near Eulipotyphla EBRs and hippocampal DEGs near breakpoints in open chromatin configurations in Soricidae, suggesting that chromosomal restructuring may influence the genomic architecture of adaptation (Fig. 1e). This could occur as rearrangements modify linkage relationships, suppress recombination, and create new regulatory relationships, thereby

maintaining advantageous allele combinations or generating novel gene interactions (Vara et al. 2021; Fernandez et al. 2024; Lin et al. 2024; Álvarez-González and Ruiz-Herrera 2025; Gompert et al. 2025). In this way, the high rate of chromosomal evolution in *S. araneus* could facilitate the retention of molecular changes underlying key traits such as brain size plasticity and high metabolic rate. Thus, rather than being merely a byproduct of genomic instability, karyotypic evolution in the common shrew may serve as an engine for diversification, adaptation, and phenotypic innovation.

Limitations

We conducted comparative analyses to characterize chromosome evolution and identify positive selection in the protein-coding genes of *S. araneus* and other species with Dehnel-like phenotypes while also examining these results in relation to seasonal and evolutionary changes in brain RNA expression. However, this study has several limitations. To determine if the Radolfzell population is a distinct chromosomal race requires additional cytogenetic verification. Currently, the identification of large-scale adaptive genomic changes (eg gene family expansions, contractions, and indel analyses) in Eulipotyphla is limited by challenges in gene annotation. TOGA, one of the most reliable annotation tools available, exhibits reduced accuracy in Eulipotyphlans relative to other mammalian lineages (Kirilenko et al. 2023), making these analyses premature until improved assemblies and pipelines become available. Additionally, while protein-coding genes are essential, they are not the sole contributors to phenotypic information within the genome (Duret et al. 1993). A significant portion of the vertebrate genome is noncoding, consisting of conserved noncoding elements (CNEs) and cis-regulatory elements (CREs) that play crucial regulatory roles in gene expression, including in brain development (Zhuang et al. 2023) and in alternative wintering strategies (Nakayama and Makino 2024). As we explore gene regulation associated with Dehnel's phenomenon across diverse tissues, future studies should investigate the evolution of common shrew CNEs and CREs, which will become more feasible as more chromosome-level genome assemblies of Eulipotyphlans are sequenced.

Lastly, future mechanistic experiments can test both functional and evolutionary hypotheses generated from these analyses. For example, *in vitro* perturbation assays in common shrew neural cell lines or organoids could be used to examine how candidate genes influence neurogenesis and cellular differentiation. Similarly, targeted manipulations in brain microvascular endothelial cells, astrocytes, or pericytes could reveal the role of genes such as *VEGFA* and *SPHK2* in regulating blood–brain barrier integrity. These approaches would help establish causal links between our proposed molecular mechanisms and the phenotypic adaptations associated with Dehnel's phenomenon.

Conclusion

S. araneus has evolved a unique set of traits, including a high rate of chromosomal rearrangements and more seasonal brain size plasticity than any other mammal. Yet, the impacts of both selection on protein-coding genes and gene regulation on these traits were unknown. We therefore generated a chromosome-level genome assembly and conducted comparative genomics and seasonal transcriptomic analyses, with three key findings. First, genes and pathways involved in neurogenesis (*SOX9*, Notch signaling, *PCDHA6*) appear critical to the evolution and regulation of Dehnel's phenomenon, suggesting that processes related to adult neurogenesis may mitigate the negative effects of changing brain size. Second, genes previously identified as upregulated in the *S. araneus* hypothalamus were also under positive selection in *S. araneus* (*VEGFA*, *SPHK2*), highlighting potential synergies between protein-coding and expression adaptations to improve metabolic homeostasis in Dehnel's phenomenon. Third, PSGs enrich the Fanconi anemia DNA repair pathway (*FANCI*, *FAAP100*, *PALB2*) and EBRs, which we propose links increased chromosomal rearrangements and adaptive evolution in the Eurasian common shrew.

Materials and methods

Genome sequencing and assembly

A single juvenile, female European common shrew (*S. araneus*) was sampled to generate a highly contiguous reference genome from a population in Radolfzell, Germany (47.9684 N, 8.9761 E) under protocols authorized by Regierungspräsidium Freiburg, Baden-Württemberg (35-9185.81/G-19/131). While we attempted to sequence a male, the prepubescent individual was mis-sexed. This shrew was then euthanized and subsampled into tissues that were immediately flash frozen using liquid nitrogen and then stored at −80 °C until DNA extraction. Nucleic acid extraction, genome sequencing, and assembly were conducted by the Vertebrate Genomes Laboratory (pipeline v2.0), described below with specific parameters found in the VGP code repository. High-molecular-weight (HMW) DNA was extracted from spleen tissue using the Bionano Prep Animal Tissue DNA Isolation Kit according to manufacturer protocols. HMW DNA was used to prepare libraries for three sequencing types from listed kits: (i) SMRTbell Template Prep Kit for PacBio Sequel II HiFi, (ii) Bionano Prep Labelling NLRS for Bionano Genomics DLS optical mapping, and (iii) Arima-HiC kit for Arima Hi-C v2 chromatin interactions. Following sequencing, initial sequencing metrics were assessed with GenomeScope (Vurture et al. 2017). Contigs were generated by assembling and phasing PacBio reads with Hifiasm (v0.15.4) (Cheng et al. 2021). Duplications representing heterozygous contigs were identified and reassigned with the purge duplications workflow (v.1.2.5) (Guan et al. 2020). Contigs were then scaffolded using Bionano optical maps with Bionano Solve (v.3.6.1). The assembly was further assembled into chromosomal-level scaffolds with Hi-C chromatin interaction data using SALSA2 (v2.2) (Ghurye et al. 2019), followed by manual curation for errors with gEVAL (Chow et al. 2016). Assembly metrics were benchmarked throughout the pipeline using Merqury (v1.1) (Rhie et al. 2020), Quast (v5.0.2) (Gurevich et al. 2013), and BUSCO (v3.0.2) (Waterhouse et al. 2018).

Genome annotation and alignment

Gene annotation and orthology inference for *S. araneus* and *Mustela nigripes* were predicted with projections from the human

genome. First, curated assemblies of these two species were masked for repetitive regions through the creation of a de novo repeat library with RepeatModeler (v2.0.2) (Smit and Hubley) followed by "-soft" masking with RepeatMasker (v4.1.2) (Smit *et al.*). Masked genomes were then pairwise aligned to the human reference genome (hg38) using lastz (v1.04.15) with the following alignment parameters: BLASTZ_O = 400, BLASTZ_E = 30, BLASTZ_M = 254, and chainLinearGap = loose. The sensitivity and specificity of generated pairwise whole-genome alignments were improved using RepeatFiller (v1.0) with default parameters (Osipova et al. 2019) and chainCleaner (Suarez et al. 2017) with "-linearGap = medium." Resultant alignment chains were then used as inputs to predict orthologous gene locations with TOGA (v1.0) (Kirilenko et al. 2023), with cluster memory bins set at 10, 100, and 268 GB (maximum memory available on our cluster). Annotation completeness for both species was then assessed with BUSCO v5.2.2 (Waterhouse et al. 2018) in comparison to mammalia_odb10.

S. araneus and *M. nigripes* TOGA annotations were then aligned to 38 mammalian TOGA annotations acquired from https://genome.senckenberg.de//download/TOGA/, including the stoat (*M. erminea*), the domesticated ferret (*M. putorius furo*), and the pygmy shrew (*S. etruscus*), all of which also undergo Dehnel-like growth patterns. Aligned species were chosen to reduce overrepresentation of species in orders or superorders (7 Eulipotyphlans, 4 Chiropterans, 6 Artiodactyls, 1 Perissodactyl, 1 Pholidota, 8 Carnivorans, 6 Glires, 6 Primates, 1 Scandentia), with genome annotations by TOGA requiring >16,000 annotated genes with BUSCOs >80% (Supplementary material). The longest transcript for each gene was selected and aligned using the MACSE exon-by-exon alignment function of TOGA to produce multiple codon alignments, with the max copies parameter set to 1. These alignments were cleaned with TAPER (v1.0.0) default settings (Zhang et al. 2021) using Julia (v 1.9.4) (Bezanson et al. 2024). Species were removed from each codon alignment prior to selection analyses when multiple copies of the gene were present or the alignment contained a frameshift, with codon alignments including at least 60% of the species (>24) retained for selection analyses.

Selection models

To infer positive selection for lineages within the phylogeny, we used the adaptive branch-site random effects likelihood (aBSREL v2.2) model (Smith et al. 2015) implemented in Hypothesis Testing using Phylogenies (HYPHY) (v2.5.32) (Kosakovsky Pond et al. 2020). First, tree pruning was conducted using an ETE Toolkit python wrapper (v3) (Huerta-Cepas et al. 2016), wherein unrooted trees for each codon alignment were pruned from a larger Bayesian molecular-clock mammalian phylogeny (Álvarez-Carretero et al. 2022). Multiple aBSREL tests were run. Branch-site models were used to infer positive selection in genes for a priori foreground lineage, including *S. araneus*, and those with Dehnel-like phenotypes (*M. erminea*, *M. putorius furo*, *S. etruscus*). Then, we conducted an exploratory analysis in which all background branches were tested for potential positive selection. This step identified genes evolving under positive selection outside of the focal species to test for lineage specificity. To test if genes significantly rejected the null hypothesis of no positive selection, we conducted a likelihood ratio test (LRT), with *P*-values quantified using a chi-squared distribution (χ^2_1) and adjusted for multiple hypothesis tests across genes and species with Holm–Bonferroni corrections (significant when $P_{adj} < 0.05$).

Running both a priori and exploratory analyses allows identifying genes under positive selection in *S. araneus* (regardless of phylogeny-wide selection), genes under positive selection strictly in *S. araneus* (no other branches with positive selection), and genes evolving in parallel related to Dehnel's phenomenon (under positive selection in *S. araneus*, two other foreground lineages, <5 other background lineages). To detect potential functional parallelism underlying seasonal size plasticity, we ran a gene set enrichment analysis on our entire candidate gene set, including both total *S. araneus*- and *S. araneus*-specific PSGs, using the DAVID functional annotation tool (Huang et al. 2009) with KEGG gene ontologies (GOs) and functional annotations. Finally, we used MEME (v2.1.2) (Murrell et al. 2012) analyses to detect which codons show signals of positive selection per gene using lineages with inferred positive selection. Here, we used a higher threshold for significance ($P < 0.1$) because MEME is a conservative test wherein the null model is based on the assumption that all sites evolve neutrally, as recommended by HyPhy (Kosakovsky Pond et al. 2020), while also applying a strict empirical Bayes factor threshold (EBF > 100).

Chromosomal evolution

Structural variant analysis of *S. araneus* and ancestral karyotype reconstruction of Eulipotyphla were conducted with DESCHRAMBLER (v1) (Kim et al. 2017). Using the new chromosome-scale *S. araneus* genome as a reference, we produced pairwise genome alignment chains and nets for five Eulipotyphla species (*C. cristata*, *G. pyrenaicus*, *S. etruscus*, *T. occidentalis*, *E. europaeus*) and two Chiropterans (*R. ferrumequinum* and *P. discolor*; outgroups) with high-quality assemblies (>5 million scaffold N50, BUSCO > 95%). Chains and nets were made with lastz as described above. Conserved segments, orthology blocks, and predicted ancestral chromosome structure were identified by DESCHRAMBLER with a 1 Mb resolution parameter and visualized using syntenyPlotteR (Quigley et al. 2023).

Transcriptomics

Transcriptomic data for the cortex and hippocampus were used to explore the regulatory mechanisms of brain shrinkage and regrowth through Dehnel's phenomenon and identify further overlap with PSGs. These regions were selected based on both empirical evidence and their functional relevance to seasonal behavioral adaptation. The cortex exhibits the largest absolute change in volume between seasons, making it a critical region for studying the molecular basis of extreme brain plasticity (Lázaro et al. 2018a; Baldoni et al. 2025b). The hippocampus was included because of its close functional relationship with the cortex as both regions are important for higher-order learning, spatial memory, and adaptive behavior processes, which may be essential for shrew winter survival (Lázaro et al. 2018b; Baldoni et al. 2025a). Together with previously published work analyzing the hypothalamus (Thomas et al. 2025), which regulates endocrine and metabolic functions, these datasets extend the framework for understanding seasonal remodeling across diverse brain regions in the common shrew.

Although shrew size change can be reproduced in seminatural conditions (Lázaro et al. 2019; Baldoni et al. 2025a), recent work demonstrates that captivity substantially alters brain gene expression profiles (Bedoya Duque et al. 2025). Such effects likely arise from differences in lifestyle, diet, and environmental enrichment, which may cause chronic stress and mask or distort the natural physiological responses that occur in the wild (Baldoni et al. 2025a). For this reason, we used a natural experimental design comparing wild individuals across seasons, capturing gene expression changes associated with environmental shifts, particularly temperature fluctuations and resource limitation, rather than confounded responses to laboratory housing.

Shrews were sampled, brain regions dissected, and RNA extracted as described in previous studies (Thomas et al. 2025, 2026). Briefly, common shrews were collected (n = 24) across five seasons (n = 4 to 5/season) of Dehnel's phenomenon (summer juveniles, autumn, winter, spring, summer adults) from a single German population (47.9684 N, 8.9761 E) using a protocol that minimized trap-related stress and hunger. Sex, sampling date, and body mass of each shrew can be found in Data S5. Shrews were euthanized with vascular perfusion of PAXgene Tissue Fixative, with brain regions dissected in cold fixative. The cortex and hippocampus were incubated in PAXgene Tissue Stabilizer for 2 to 24 h and snap frozen in liquid nitrogen (−180 °C). RNA was extracted from each region using a modified Qiagen Micro RNAeasy protocol designed for small amounts of mammalian sensory tissue to reduce heat-associated RNA degradation. Quality control (nanodrop and RNA ScreenTape), library preparation (poly-A selection), and sequencing (approx. 15 to 25 million reads/sample, 150 bp PE) was conducted by Azenta Life Sciences. No technical replicates were used in these analyses.

For each sample, raw reads were trimmed for adapter sequences and pruned for low-quality sequences using fastp (Chen et al. 2018) and then aligned to the novel NCBI *S. araneus* transcriptome (GCF_027595985.1_mSorAra2.pri_rna.fna) using Kallisto (v0.46.2) (Bray et al. 2016), both with default parameters. Counts were normalized using the DESeq2 (v1.36) (Love et al. 2014) median of ratios that accounts for library size and content. We then tested for differential expression in both regions between autumn and spring individuals. These seasons were chosen as they resemble the shrinking and regrowth phases of Dehnel's phenomenon and were previously analyzed in the hypothalamus (Thomas et al. 2025). Genes were tested for differential expression ($P_{adj} < 0.05$) using a Wald test in DESeq2 (Love et al. 2014), with sex as an additional covariate (∼sex + season), followed by Benjamini–Hochberg multiple test correction (Benjamini and Hochberg 1995). We then ran a KEGG GO enrichment using fgsea (v1.22) (Korotkevich et al. 2021) with default parameters to describe potential molecular functions or pathways associated with identified differential expression ($P_{adj} < 0.05$). Lastly, we identified genes that overlapped with genes inferred to be evolving under positive selection.

Multiassociation analysis

RegioneR (v1.26) (Gel et al. 2016) was used to calculate statistical associations between different genomic features as previously described (Álvarez-González et al. 2022a, 2022b, ; Marín-Gual et al. 2025). Pairwise associations were represented as heatmaps with *z*-score values higher than 0 indicating a positive association between the two analyzed features and *z*-score values lower than 0 indicating a negative association (adjusted $P < 0.05$ in both cases). *Z*-score values equal to 0 indicate no statistically significant association between the two features (adjusted $P > 0.05$). For the multiassociation analysis, A/B compartments, TADs, their boundaries, DEGs, and PSGs were included. A/B compartments were called from normalized matrices at a 500 Kbp resolution using the package FAN-C (v0.9.14) and TADs were called using the function find_tads from TADbit (Serra et al. 2017).

Acknowledgments

Bioinformatic analyses were conducted on UMass Amherst's Unity HPC cluster. Additionally, we thank Marion Muturi for the support with fieldwork. The authors would like to thank Stony Brook Research Computing and Cyberinfrastructure and the Institute for Advanced Computational Science at Stony Brook University for access to the high-performance SeaWulf computing system, which was made possible by $1.85M in grants from the National Science Foundation (awards 1531492 and 2215987) and matching funds from the the Empire State Development's Division of Science, Technology and Innovation (NYSTAR) program (contract C210148).

Author contributions

William R. Thomas (Conceptualization, Data curation, Formal analysis, Investigation, Methodology, Validation, Visualization, Writing—original draft), Tanya M. Lama (Methodology, Software, Resources, Writing—review & editing), Cecilia Baldoni (Data curation), Laia Marín-Gual (Formal analysis, Methodology, Writing—review & editing), Diana Moreno Santillán (Methodology, Writing—review & editing), Marta Farré (Methodology, Software), Linelle Abueg (Data curation), Jennifer Balacco (Data curation), Olivier Fedrigo (Methodology), Giulio Formenti (Methodology, Supervision, Visualization, Writing—review & editing), Nivesh Jain (Data curation), Jacquelyn Mountcastle (Data curation), Tatiana Tilley (Data curation), Dominik von Elverfeldt (Writing—review & editing), John Nieland (Funding acquisition, Writing—review & editing), Angelique P. Corthals (Funding acquisition, Investigation, Writing—review & editing), Aurora Ruiz-Herrera (Methodology, Writing—review & editing), Dina K.N. Dechmann (Funding acquisition, Writing—review & editing), Erich Jarvis (Supervision, Writing—review & editing), Liliana M. Dávalos (Conceptualization, Funding acquisition, Project administration, Supervision, Writing—review & editing), David A. Ray (Writing—review & editing), and AA (Data curation)

Supplementary material

Supplementary material is available at *Molecular Biology and Evolution* online.

Funding

This work was supported by the Human Frontiers of Science Program, award: RGP0013/2019 (to DKND, JN, and LMD); a Stony Book University Presidential Innovation and Excellence award (to

LMD) and the U.S. National Science Foundation (NSF) through DBI 2010853 (to TL); DEB 1838273, IOS 2031906 and 2032063 (to LMD); IOS 2031926 and 2032011 (to APC); and IOS 2032006 and DEB 1838283 (to DAR); the Spanish Ministry of Science and Innovation (PID2020-112557GB-I00 founded by AEI/10.13039/501100011033 to AR-H); the Agència de Gestió d'Ajuts Universitaris i de Recerca, AGAUR (2021SGR00122 to AR-H); the Catalan Institution for Research and Advanced Studies (ICREA Academia to AR-H); and an FPU predoctoral fellowship from the Ministry of Science, Innovation and University (FPU18/03867 to LM-G).

Conflicts of interests

All other authors declare they have no competing interests.

Data availability

All data are available in the main text or the Supplementary materials. Cleaned whole-genome alignments, cleaned gene alignments, and selection outputs are openly available on Dryad (https://doi.org/10.5061/dryad.8gtht770x). Supplementary tables, results, and codes are deposited and found on GitHub (https://github.com/wrthomas315/Sorex_Genome2). Raw sequencing data are located in the NCBI Sequencing Read Archive (BioProject PRJNA941271). BioRender was used to generate Fig. 1, and ChatGPT was sparingly used to improve manuscript grammar.

References

Ables JL, Breunig JJ, Eisch AJ, Rakic P. Not(ch) just development: notch signalling in the adult brain. *Nat Rev Neurosci*. 2011:12:269–283. https://doi.org/10.1038/nrn3024.

Alcón P *et al.* FANCD2–FANCI is a clamp stabilized on DNA by monoubiquitination of FANCD2 during DNA repair. *Nat Struct Mol Biol*. 2020:27:240–248. https://doi.org/10.1038/s41594-020-0380-1.

Alcón P *et al.* FANCD2–FANCI surveys DNA and recognizes double- to single-stranded junctions. *Nature*. 2024:632:1165–1173. https://doi.org/10.1038/s41586-024-07770-w.

Álvarez-Carretero S *et al.* A species-level timeline of mammal evolution integrating phylogenomic data. *Nature*. 2022:602:263–267. https://doi.org/10.1038/s41586-021-04341-1.

Álvarez-González L *et al.* Principles of 3D chromosome folding and evolutionary genome reshuffling in mammals. *Cell Rep*. 2022a:41:111839. https://doi.org/10.1016/j.celrep.2022.111839.

Álvarez-González L *et al.* 3D chromatin remodelling in the germ line modulates genome evolutionary plasticity. *Nat Commun*. 2022b:13:2608. https://doi.org/10.1038/s41467-022-30296-6.

Álvarez-González L, Ruiz-Herrera A. Evolution of 3D chromatin folding. *Annu Rev Anim Biosci*. 2025:13:49–71. https://doi.org/10.1146/annurev-animal-111523-102233.

Apfelbach R, Kruska D. Zur postnatalen Hirnentwicklung beim Frettchen *Mustela putorius* f. furo (Mustelidae; Mammalia). *Z. Säugetierkd*. 1979:44(2):127–131. https://archive.org/download/mammalian-biology_1979_44_contents/mammalian-biology_1979_44_contents.pdf.

Arcondéguy T, Lacazette E, Millevoi S, Prats H, Touriol C. VEGF-A mRNA processing, stability and translation: a paradigm for intricate regulation of gene expression at the post-transcriptional level. *Nucleic Acids Res*. 2013:41:7997–8010. https://doi.org/10.1093/nar/gkt539.

Artavanis-Tsakonas S, Rand MD, Lake RJ. Notch signaling: cell fate control and signal integration in development. *Science*. 1999:284:770–776. https://doi.org/10.1126/science.284.5415.770.

Baldoni C *et al.* Captivity alters behaviour but not seasonal brain size change in semi-naturally housed shrews. *R Soc Open Sci*. 2025a:12:242138. https://doi.org/10.1098/rsos.242138.

Baldoni C *et al.* Programmed seasonal brain shrinkage in the common shrew via water loss without cell death. *Curr Biol*. 2025b:35:4642–4650.e3. https://doi.org/10.1016/j.cub.2025.08.015.

Bardhan A, Sharma T. Meiosis and speciation: a study in a speciating Mus terricolor complex. *J Genet*. 2000:79:105–111. https://doi.org/10.1007/BF02715858.

Bedoya Duque MA *et al.* Gene expression comparisons between captive and wild shrew brains reveal captivity effects. *Biol Lett*. 2025:21:20240478. https://doi.org/10.1098/rsbl.2024.0478.

Benathar TCM *et al.* Karyotype, evolution and phylogenetic reconstruction in Micronycterinae bats with implications for the ancestral karyotype of Phyllostomidae. *BMC Evol Biol*. 2019:19:98. https://doi.org/10.1186/s12862-019-1421-4.

Benjamini Y, Hochberg Y. Controlling the false discovery rate: a practical and powerful approach to multiple testing. *J R Stat Soc*. 1995:57:289–300. https://doi.org/10.1111/j.2517-6161.1995.tb02031.x.

Bezanson J, Karpinski S, Shah VB, Edelman A. 2024. Julia: A Fast Dynamic Language for Technical Computing [preprint]. arXIv 1–27. https://doi.org/10.48550/arXiv.1209.5145.

Bray NL, Pimentel H, Melsted P, Pachter L. Near-optimal probabilistic RNA-seq quantification. *Nat Biotechnol*. 2016:34:525–527. https://doi.org/10.1038/nbt.3519.

Brosh RMJ, Bellani M, Liu Y, Seidman MM. Fanconi Anemia: a DNA repair disorder characterized by accelerated decline of the hematopoietic stem cell compartment and other features of aging. *Ageing Res Rev*. 2017:33:67–75. https://doi.org/10.1016/j.arr.2016.05.005.

Bruère AN. 1975. The discovery and biological consequences of some important chromosome anomalies in populations of domestic animals. Proceedings of 1st World Congress on Genetics Applied to Livestock Production; Editorial Garsi; Madrid, Spain. p. 151–175.

Cardoso-Moreira M *et al.* Gene expression across mammalian organ development. *Nature*. 2019:571:505–509. https://doi.org/10.1038/s41586-019-1338-5.

Chapouton P *et al.* Notch activity levels control the balance between quiescence and recruitment of adult neural stem cells. *J Neurosci*. 2010:30:7961–7974. https://doi.org/10.1523/JNEUROSCI.6170-09.2010.

Chen S, Zhou Y, Chen Y, Gu J. Fastp: an ultra-fast all-in-one FASTQ preprocessor. *Bioinformatics*. 2018:34:i884–i890. https://doi.org/10.1093/bioinformatics/bty560.

Chen WV *et al.* Pcdhαc2 is required for axonal tiling and assembly of serotonergic circuitries in mice. *Science*. 2017:356:406–411. https://doi.org/10.1126/science.aal3231.

Cheng H, Concepcion GT, Feng X, Zhang H, Li H. Haplotype-resolved de novo assembly using phased assembly graphs with hifiasm. *Nat Methods*. 2021:18:170–175. https://doi.org/10.1038/s41592-020-01056-5.

Cheng LC, Pastrana E, Tavazoie M, Doetsch F. MiR-124 regulates adult neurogenesis in the subventricular zone stem cell niche. *Nat Neurosci*. 2009:12:399–408. https://doi.org/10.1038/nn.2294.

Chow W *et al.* GEVAL—A web-based browser for evaluating genome assemblies. *Bioinformatics*. 2016:32:2508–2510. https://doi.org/10.1093/bioinformatics/btw159.

Christensen K, Johnson TE, Vaupel JW. The quest for genetic determinants of human longevity: challenges and insights. *Nat Rev Genet*. 2006:7:436–448. https://doi.org/10.1038/nrg1871.

Churchfield S, Rychlik L, Taylor JRE. Food resources and foraging habits of the common shrew, Sorex araneus: does winter food shortage explain Dehnel's phenomenon? *Oikos*. 2012:121:1593–1602. https://doi.org/10.1111/j.1600-0706.2011.20462.x.

Crombach A, Hogeweg P. Chromosome rearrangements and the evolution of genome structuring and adaptability. *Mol Biol Evol*. 2007:24:1130–1139. https://doi.org/10.1093/molbev/msm033.

Csukasi F *et al.* Dominant-negative SOX9 mutations in campomelic dysplasia. *Hum Mutat*. 2019:40:2344–2352. https://doi.org/10.1002/humu.23888.

Dean R, Harrison PW, Wright AE, Zimmer F, Mank JE. Positive selection underlies Faster-Z evolution of gene expression in birds. *Mol Biol Evol*. 2015:32:2646–2656. https://doi.org/10.1093/molbev/msv138.

Debrabant B *et al.* Human longevity and variation in DNA damage response and repair: study of the contribution of sub-processes using competitive gene-set analysis. *Eur J Hum Genet*. 2014:22:1131–1136. https://doi.org/10.1038/ejhg.2013.299.

Dehnel A. Studies of the genus *Sorex* L. *Ann Univ M Curie-Sklod*. 1949:4:17–104.

Dubey S, Salamin N, Ohdachi SD, Barrière P, Vogel P. Molecular phylogenetics of shrews (Mammalia: Soricidae) reveal timing of transcontinental colonizations. *Mol Phylogenet Evol*. 2007:44:126–137. https://doi.org/10.1016/j.ympev.2006.12.002.

Duret L, Dorkeld F, Gautier C. Strong conservation of non-coding sequences during vertebrates evolution: potential involvement in post-transcriptional regulation of gene expression. *Nucleic Acids Res*. 1993:21:2315–2322. https://doi.org/10.1093/nar/21.10.2315.

Fernandez R, *et al.* 2024. A punctuated burst of massive genomic rearrangements by chromosome shattering and the origin of non-marine annelids [preprint]. Research Square. https://doi.org/10.21203/rs.3.rs-4346819/v1.

Fukuda N *et al.* Axonal mRNA binding of hnRNP A/B is crucial for axon targeting and maturation of olfactory sensory neurons. *Cell Rep*. 2023:42:112398. https://doi.org/10.1016/j.celrep.2023.112398.

Galindo DJ *et al.* Chromosomal polymorphism and speciation: the case of the genus mazama (cetartiodactyla; cervidae). *Genes (Basel)*. 2021:12:165. https://doi.org/10.3390/genes12020165.

Garagna S, Page J, Fernandez-Donoso R, Zuccotti M, Searle JB. The robertsonian phenomenon in the house mouse: mutation, meiosis and speciation. *Chromosoma*. 2014:123:529–544. https://doi.org/10.1007/s00412-014-0477-6.

Gel B *et al.* Regioner: an R/Bioconductor package for the association analysis of genomic regions based on permutation tests. *Bioinformatics*. 2016:32:289–291. https://doi.org/10.1093/bioinformatics/btv562.

Ghurye J *et al.* Integrating Hi-C links with assembly graphs for chromosome-scale assembly. *PLoS Comput Biol*. 2019:15:e1007273. https://doi.org/10.1371/journal.pcbi.1007273.

Gomes AJB *et al.* Karyotypic variation in Rhinophylla pumilio Peters, 1865 and comparative analysis with representatives of two subfamilies of Phyllostomidae (Chiroptera). *Comp Cytogenet*. 2012:6:213–225. https://doi.org/10.3897/compcytogen.v6i2.1679.

Gompert Z *et al.* Adaptation repeatedly uses complex structural genomic variation. *Science*. 2025:388:eadp3745. https://doi.org/10.1126/science.adp3745.

Guan D *et al.* Identifying and removing haplotypic duplication in primary genome assemblies. *Bioinformatics*. 2020:36:2896–2898. https://doi.org/10.1093/bioinformatics/btaa025.

Guo Y, Feng W, Sy SMH, Huen MSY. ATM-dependent phosphorylation of the fanconi anemia protein PALB2 promotes the DNA damage response. *J Biol Chem*. 2015:290:27545–27556. https://doi.org/10.1074/jbc.M115.672626.

Gurevich A, Saveliev V, Vyahhi N, Tesler G. QUAST: quality assessment tool for genome assemblies. *Bioinformatics*. 2013:29:1072–1075. https://doi.org/10.1093/bioinformatics/btt086.

Hashimoto-Torii K *et al.* Interaction between reelin and notch signaling regulates neuronal migration in the cerebral Cortex. *Neuron*. 2008:60:273–284. https://doi.org/10.1016/j.neuron.2008.09.026.

Healy K *et al.* Ecology and mode-of-life explain lifespan variation in birds and mammals. *Proc Biol Sci.* 2014:281:20140298. https://doi.org/10.1098/rspb.2014.0298.

Huang DW, Sherman BT, Lempicki RA. Systematic and integrative analysis of large gene lists using DAVID bioinformatics resources. *Nat Protoc*. 2009:4:44–57. https://doi.org/10.1038/nprot.2008.211.

Huerta-Cepas J, Serra F, Bork P. ETE 3: reconstruction, analysis, and visualization of phylogenomic data. *Mol Biol Evol*. 2016:33:1635–1638. https://doi.org/10.1093/molbev/msw046.

Hyvärinen H. Wintering strategy of voles and shrews in Findland. *Winter Ecol Small Mamm*. 1984:10:139–148.

Keicher L, O'Mara MT, Voigt CC, Dechmann DKN. Stable carbon isotopes in breath reveal fast metabolic incorporation rates and seasonally variable but rapid fat turnover in the common shrew (Sorex araneus). *J Exp Biol*. 2017:220:2834–2841. https://doi.org/10.1242/jeb.159947.

Khaitovich P *et al.* Parallel patterns of evolution in the genomes and transcriptomes of humans and chimpanzees. *Science*. 2005:309:1850–1854. https://doi.org/10.1126/science.1108296.

Khaitovich P, Enard W, Lachmann M, Pääbo S. Evolution of primate gene expression. *Nat Rev Genet*. 2006:7:693–702. https://doi.org/10.1038/nrg1940.

Kim J *et al.* Reconstruction and evolutionary history of eutherian chromosomes. *Proc Natl Acad Sci U S A*. 2017:114:E5379–E5388. https://doi.org/10.1073/pnas.1702012114.

Kirilenko BM *et al.* Integrating gene annotation with orthology inference at scale. *Science*. 2023:380:eabn3107. https://doi.org/10.1126/science.abn3107.

Korotkevich G, Sukhov V, Budin N, Atryomov MN, Sergushichev A. 2021. Fast gene set enrichment analysis [preprint]. bioRxiv. https://www.biorxiv.org/content/10.1101/060012v3.abstract.

Kosakovsky Pond SL *et al.* Hyphy 2.5—A customizable platform for evolutionary hypothesis testing using phylogenies. *Mol Biol Evol*. 2020:37:295–299. https://doi.org/10.1093/molbev/msz197.

Küsters B *et al.* Differential effects of vascular endothelial growth factor A isoforms in a mouse brain metastasis model of human melanoma. *Cancer Res*. 2003:63:5408–5413. PMID: 14500375.

Kwok C *et al.* Mutations in SOX9, the gene responsible for campomelic dysplasia and autosomal sex reversal. *Am J Hum Genet*. 1995:57:1028–1036. PMID: 7485151.

Lapoint S, Keicher L, Wikelski M, Zub K, Dechmann DKN. Growth overshoot and seasonal size changes in the skulls of two weasel species. *R Soc Open Sci*. 2017:4:160947. https://doi.org/10.1098/rsos.160947.

Lázaro J *et al.* Cognitive skills of common shrews (Sorex araneus) vary with seasonal changes in skull size and brain mass. *J Exp Biol*. 2018b:221:eb166595. https://doi.org/10.1242/jeb.166595.

Lázaro J, Dechmann DKN. Dehnel's phenomenon. *Curr Biol*. 2021:31:R463–R465. https://doi.org/10.1016/j.cub.2021.04.006.

Lázaro J, Hertel M, Muturi M, Dechmann DKN. Seasonal reversible size changes in the braincase and mass of common shrews are flexibly modified by environmental conditions. *Sci Rep*. 2019:9:2489. https://doi.org/10.1038/s41598-019-38884-1.

Lázaro J, Hertel M, Sherwood CC, Muturi M, Dechmann DKN. Profound seasonal changes in brain size and architecture in the common shrew. *Brain Struct Funct*. 2018a:223:2823–2840. https://doi.org/10.1007/s00429-018-1666-5.

Lemos B, Bettencourt BR, Meiklejohn CD, Hartl DL. Evolution of proteins and gene expression levels are coupled in Drosophila and are independently associated with mRNA abundance, protein length, and number of protein-protein interactions. *Mol Biol Evol*. 2005a:22:1345–1354. https://doi.org/10.1093/molbev/msi122.

Lemos B, Meiklejohn CD, Cáceres M, Hartl DL. Rates of divergence in gene expression profiles of primates, mice, and flies: stabilizing selection and variability among functional categories. *Evolution*. 2005b:59:126–137. https://doi.org/10.1111/j.0014-3820.2005.tb00900.x.

Lin CY *et al.* Chromosome-level genome assemblies of 2 hemichordates provide new insights into deuterostome origin and chromosome evolution. *PLoS Biol*. 2024:22:e3002661. https://doi.org/10.1371/journal.pbio.3002661.

Ling C *et al.* FAAP100 is essential for activation of the Fanconi anemia-associated DNA damage response pathway. *EMBO J*. 2007:26:2104–2114. https://doi.org/10.1038/sj.emboj.7601666.

Liu H *et al.* Sphingosine kinase type 2 is a putative BH3-only protein that induces apoptosis. *J Biol Chem*. 2003:278:40330–40336. https://doi.org/10.1074/jbc.M304455200.

Love MI, Huber W, Anders S. Moderated estimation of fold change and dispersion for RNA-seq data with DESeq2. *Genome Biol*. 2014:15:550. https://doi.org/10.1186/s13059-014-0550-8.

Maceyka M *et al.* Sphk1 and SphK2, sphingosine kinase isoenzymes with opposing functions in sphingolipid metabolism. *J Biol Chem*. 2005:280:37118–37129. https://doi.org/10.1074/jbc.M502207200.

MacRae SL *et al.* DNA repair in species with extreme lifespan differences. *Aging (Albany NY)*. 2015:7:1171–1184. https://doi.org/10.18632/aging.100866.

Marín-García C *et al.* Multiple genomic landscapes of recombination and genomic divergence in wild populations of house mice—the role of chromosomal fusions and Prdm9. *Mol Biol Evol*. 2024:41:msae063. https://doi.org/10.1093/molbev/msae063.

Marín-Gual L *et al.* Meiotic cohesin RAD21L shapes 3D genome structure and transcription in the male germline. *Sci Adv*. 2025:11:eadv2283. https://doi.org/10.1126/sciadv.adv2283.

Møller OM, *et al.* Chromosomal polymorphism in the blue fox (*Alopex lagopus*) and its effects on fertility. *Hereditas*. 1985:102:159–164. https://doi.org/10.1111/j.1601-5223.1985.tb00609.x.

Murrell B *et al.* Detecting individual sites subject to episodic diversifying selection. *PLoS Genet*. 2012:8:e1002764. https://doi.org/10.1371/journal.pgen.1002764.

Nakayama D, Makino T. Convergent accelerated evolution of mammal-specific conserved non-coding elements in hibernators. *Sci Rep*. 2024:14:11754. https://doi.org/10.1038/s41598-024-62455-8.

Nováková L, Lázaro J, Muturi M, Dullin C, Dechmann DKN. Winter conditions, not resource availability alone, may drive reversible seasonal skull size changes in moles. *R Soc Open Sci*. 2022:9:220652. https://doi.org/10.1098/rsos.220652.

Nuzhdin SV, Wayne ML, Harmon KL, McIntyre LM. Common pattern of evolution of gene expression level and protein sequence in Drosophila. *Mol Biol Evol*. 2004:21:1308–1317. https://doi.org/10.1093/molbev/msh128.

Ochocińska D, Taylor JRE. Living at the physiological limits: field and maximum metabolic rates of the common shrew (Sorex araneus). *Physiol Biochem Zool*. 2005:78:808–818. https://doi.org/10.1086/431190.

Osipova E, Hecker N, Hiller M. RepeatFiller newly identifies megabases of aligning repetitive sequences and improves annotations of conserved non-exonic elements. *Gigascience*. 2019:8:giz132. https://doi.org/10.1093/gigascience/giz132.

Pritchett J, Athwal V, Roberts N, Hanley NA, Hanley KP. Understanding the role of SOX9 in acquired diseases: lessons from development. *Trends Mol Med*. 2011:17:166–174. https://doi.org/10.1016/j.molmed.2010.12.001.

Pucek Z. Seasonal and age changes in the weight of internal organs of shrews. *Acta Theriol*. 1965:10:369–438. https://doi.org/10.4098/AT.arch.65-31.

Pucek Z. Seasonal and age change in shrews as an adaptive process. In: Berry RJ, Southern HN, editors. Variation in mammalian populations the proceedings of a symposium held at the Zoological Society of London on 14 and 15 November, 1969. Published for the Zoological Society of London by Academic Press; 1970. p. 189–207.

Quigley S, Damas J, Larkin DM, Farré M. syntenyPlotteR: a user-friendly R package to visualize genome synteny, ideal for both experienced and novice bioinformaticians. *Bioinforma Adv*. 2023:3:vbad161. https://doi.org/10.1093/bioadv/vbad161.

Ray S *et al.* Seasonal plasticity in the adult somatosensory cortex. *Proc Natl Acad Sci U S A*. 2020:117:32136–32144. https://doi.org/10.1073/pnas.1922888117.

Reid S *et al.* Biallelic mutations in PALB2 cause Fanconi anemia subtype FA-N and predispose to childhood cancer. *Nat Genet*. 2007:39:162–164. https://doi.org/10.1038/ng1947.

Rhie A *et al.* Towards complete and error-free genome assemblies of all vertebrate species. *Nature*. 2021:592:737–746. https://doi.org/10.1038/s41586-021-03451-0.

Rhie A, Walenz BP, Koren S, Phillippy AM. Merqury: reference-free quality, completeness, and phasing assessment for genome assemblies. *Genome Biol*. 2020:21:245. https://doi.org/10.1186/s13059-020-02134-9.

Romanenko SA *et al.* Chromosome translocations as a driver of diversification in mole voles Ellobius (Rodentia, mammalia). *Int J Mol Sci*. 2019:20:4466. https://doi.org/10.3390/ijms20184466.

Ruiz-Herrera A, Farré M, Robinson TJ. Molecular cytogenetic and genomic insights into chromosomal evolution. *Heredity (Edinb)*. 2012:108:28–36. https://doi.org/10.1038/hdy.2011.102.

Schaeffer PJ *et al.* Metabolic rate in common shrews is unaffected by temperature, leading to lower energetic costs through seasonal size reduction. *R Soc Open Sci*. 2020:7:191989. https://doi.org/10.1098/rsos.191989.

Scott CE *et al.* SOX9 induces and maintains neural stem cells. *Nat Neurosci*. 2010:13:1181–1189. https://doi.org/10.1038/nn.2646.

Searle JB, Hughes JJ. Fertility cost (or sometimes a lack of it) in relation to heterozygosity for robertsonian rearrangements in mammals: a review. *Cytogenet Genome Res*. 2025:165: 272–306. https://doi.org/10.1159/000546385.

Searle JB, Zima J, Polly PD. Shrews, Chromosomes and Speciation. In: Searle JB, Zima J, Polly PD, editors. *Shrews, chromosomes and speciation*. Cambridge University Press; 2019. p. 455–462.

Sepp M *et al.* Cellular development and evolution of the mammalian cerebellum. *Nature*. 2024:625:788–796. https://doi.org/10.1038/s41586-023-06884-x.

Serra F *et al.* Automatic analysis and 3D-modelling of Hi-C data using TADbit reveals structural features of the fly chromatin colors. *PLoS Comput Biol*. 2017:13:e1005665. https://doi.org/10.1371/journal.pcbi.1005665.

Sharman GB. Chromosomes of the common shrew. *Nature*. 1956:177:941–942. https://doi.org/10.1038/177941a0.

Smit A, Hubley RM, Green P. RepeatMasker Open-4.0. http://www.repeatmasker.org.

Smit AFA, Hubley RM. RepeatModeler Open-1.0. 2008-2015. https://www.repeatmasker.org/faq.html#faq3.

Smith MD *et al.* Less is more: an adaptive branch-site random effects model for efficient detection of episodic diversifying selection. *Mol Biol Evol*. 2015:32:1342–1353. https://doi.org/10.1093/molbev/msv022.

Smogorzewska A *et al.* Identification of the FANCI protein, a monoubiquitinated FANCD2 paralog required for DNA repair. *Cell*. 2007:129:289–301. https://doi.org/10.1016/j.cell.2007.03.009.

Suarez HG, Langer BE, Ladde P, Hiller M. ChainCleaner improves genome alignment specificity and sensitivity. *Bioinformatics*. 2017:33: 1596–1603. https://doi.org/10.1093/bioinformatics/btx024.

Takasugi N *et al.* BACE1 activity is modulated by cell-associated sphingosine-1-phosphate. *J Neurosci*. 2011:31:6850–6857. https://doi.org/10.1523/JNEUROSCI.6467-10.2011.

Taylor JRE, Rychlik L, Churchfield S. Winter reduction in body mass in a very small, nonhibernating mammal: consequences for heat loss and metabolic rates. *Physiol Biochem Zool*. 2013:86:9–18. https://doi.org/10.1086/668484.

Thomas WR *et al.* Seasonal and comparative evidence of adaptive gene expression in mammalian brain size plasticity. *Elife*. 2025:13:RP100788. https://doi.org/10.7554/eLife.100788.

Thomas WR *et al.* Dynamic metabolic and molecular changes during seasonal shrinking in *Sorex araneus*. *Genome Res*. 2026:36:61–70. https://doi.org/10.1101/gr.280639.125.

Troshina A, Gustavsson I, Tikhonov VN. Investigation of two centric fusion translocations of wild pigs by different banding techniques. *Hereditas*. 1985:102:155–158. https://doi.org/10.1111/j.1601-5223.1985.tb00476.x.

Vadodaria KC *et al.* Altered serotonergic circuitry in SSRI-resistant major depressive disorder patient-derived neurons. *Mol Psychiatry*. 2019:24:808–818. https://doi.org/10.1038/s41380-019-0377-5.

Vara C *et al.* The impact of chromosomal fusions on 3D genome folding and recombination in the germ line. *Nat Commun*. 2021:12:2981. https://doi.org/10.1038/s41467-021-23270-1.

Vong KI, Leung CKY, Behringer RR, Kwan KM. Sox9 is critical for suppression of neurogenesis but not initiation of gliogenesis in the cerebellum. *Mol Brain*. 2015:8:25. https://doi.org/10.1186/s13041-015-0115-0.

Vurture GW *et al.* GenomeScope: fast reference-free genome profiling from short reads. *Bioinformatics*. 2017:33:2202–2204. https://doi.org/10.1093/bioinformatics/btx153.

Waterhouse RM *et al.* BUSCO applications from quality assessments to gene prediction and phylogenomics. *Mol Biol Evol*. 2018:35:543–548. https://doi.org/10.1093/molbev/msx319.

White TA, Bordewich M, Searle JB. A network approach to study karyotypic evolution: the chromosomal races of the common shrew (sorex araneus) and house mouse (Mus musculus) as model systems. *Syst Biol*. 2010:59:262–276. https://doi.org/10.1093/sysbio/syq004.

Wirthlin M *et al.* Parrot genomes and the evolution of heightened longevity and cognition. *Curr Biol*. 2018:28:4001–4008.e7. https://doi.org/10.1016/j.cub.2018.10.050.

Xia B *et al.* Control of BRCA2 cellular and clinical functions by a nuclear partner, PALB2. *Mol Cell*. 2006:22:719–729. https://doi.org/10.1016/j.molcel.2006.05.022.

Xia B *et al.* Fanconi anemia is associated with a defect in the BRCA2 partner PALB2. *Nat Genet*. 2007:39:159–161. https://doi.org/10.1038/ng1942.

Yagi T, Takeichi M. Cadherin superfamily genes: functions, genomic organization, and neurologic diversity. *Genes Dev*. 2000:14:1169–1180. https://doi.org/10.1101/gad.14.10.1169.

Yoon K, Gaiano N. Notch signaling in the mammalian central nervous system: insights from mouse mutants. *Nat Neurosci*. 2005:8:709–715. https://doi.org/10.1038/nn1475.

Yosida TH. Karyotypes and meiotic segregation of hybrids betwen Asian and Oceanian type black rats. *Proc Japan Acad*. 1976:52:304–307. https://doi.org/10.2183/pjab1945.52.304.

Yousefzadeh M *et al.* Dna damage—how and why we age? *Elife*. 2021:10:e62852. https://doi.org/10.7554/eLife.62852.

Zhang C, Zhao Y, Braun EL, Mirarab S. TAPER: pinpointing errors in multiple sequence alignments despite varying rates of evolution. *Methods Ecol Evol*. 2021:12:2145–2158. https://doi.org/10.1111/2041-210X.13696.

Zhuang XL *et al.* Integrative omics reveals rapidly evolving regulatory sequences driving primate brain evolution. *Mol Biol Evol*. 2023:40:msad173. https://doi.org/10.1093/molbev/msad173.